High-Affinity Binding of the Neonatal Fc Receptor to Its IgG Ligand Requires Receptor Immobilization†

Daniel E. Vaughn‡ and Pamela J. Bjorkman*,‡,§

Division of Biology 156-29 and Howard Hughes Medical Institute, California Institute of Technology, Pasadena, California 91125

Received April 10, 1997; Revised Manuscript Received May 20, 1997⊗

ABSTRACT: The neonatal Fc receptor (FcRn) binds maternal immunoglobulin G (IgG) during the acquisition of passive immunity by the fetus or newborn. In adult mammals, FcRn also binds IgG and returns it to the bloodstream, thus protecting IgG from a default degradative pathway. Biosensor assays have been used to characterize the interaction of a soluble form of FcRn with IgG. We use the statistical method of cross-validation to show that there are two classes of noninteracting binding sites, and these are sufficient to account for previously observed nonlinear Scatchard plots of FcRn/IgG binding data. We demonstrate that immobilization of FcRn on the biosensor surface reproduces the high-affinity IgG binding observed for membrane-bound FcRn, whereas immobilization of IgG results in lower affinity binding similar to that of the FcRn/IgG interaction in solution. The dependence of FcRn/IgG binding affinity on the coupled molecule provides further evidence in support of the previously hypothesized model that an FcRn dimer forms the high-affinity IgG binding site.

The neonatal Fc receptor (FcRn)[1] binds immunoglobulin G (IgG) in two important physiological processes: the transfer of IgG from mother to fetus or newborn and the protection of IgG from a default degradative pathway (reviewed in ref *1)*. FcRn is structurally similar to class I MHC molecules, consisting of a homologous membrane-bound heavy chain and the class I MHC light chain, β_2-microglobulin (*2, 3*). A soluble form of FcRn, a heterodimer composed of the extracellular domains of the heavy chain complexed to β_2-microglobulin, was previously shown to be functionally active (*4*), retaining its high-affinity IgG binding at pH 6.0 with a sharp drop in affinity at pH values above 7 (*4*−*6*).

Our laboratory has used a biosensor assay to characterize the binding of soluble FcRn to IgG (*6*−*8*). Biosensors utilize a surface plasmon resonance (SPR) based assay that allows the formation of a protein−protein complex to be monitored several times per second (*9*−*11*). In this system, one molecule is immobilized at the sensor chip surface, and binding of the second molecule is monitored as it is passed over the chip. Scatchard and kinetic analyses of the binding between FcRn and IgG were used to calculate binding affinities (*6*−*8*). These characterizations were complicated by nonlinearity of the Scatchard plots, suggesting the presence of multiple classes of binding sites.

Here, we demonstrate that the interaction of IgG with immobilized FcRn can best be modeled as IgG binding to two classes of noninteracting sites on FcRn, and describe a method to derive accurate binding constants for each class. Using this method, we show that the affinities of FcRn for different IgGs are systematically higher when FcRn, rather than the IgG, is immobilized. The affinities of immobilized FcRn for IgG are comparable to those observed in binding assays using membrane-bound FcRn (*7, 12)*, suggesting that immobilization of FcRn on a biosensor chip mimics the physiological situation. These results are interpreted with reference to previous work demonstrating that FcRn dimerization is required for high-affinity binding of IgG (*8*).

MATERIALS AND METHODS

Proteins and Reagents. Secreted rat FcRn (a heterodimer composed of residues 1−269 of the rat FcRn heavy chain associated with rat β2m) was purified from supernatants of transfected Chinese hamster ovary cells using pH-dependent binding to rat IgG affinity columns (*4*). 1B5 and 3F4 are murine IgG1 monoclonal antibodies against human Zn-α_2-glycoprotein (*13*). They were purified from ascites fluid by thiophillic adsorption on a T-gel column according to the manufacturer's protocol (Pierce Chemical Co.) and by FcRn affinity chromatography (*14*). Monoclonal mouse and rat antibodies of the specified subtypes were purchased from Pharmingen. Anti-CD4, a rat IgG2a, was purchased from Boehringer Mannheim. Polyclonal human IgG and Fc fragments (Hu IgG and Hu Fc; mixture of IgG1, IgG2, IgG3, and IgG4 subtypes) and polyclonal rat IgG and Fc fragments (mixture of IgG1, IgG2a, IgG2b, and IgG2c subtypes) were purchased from Jackson ImmunoResearch.

Protein concentrations were determined spectrophotometrically using extinction coefficients at 280 nm of 216 000 M^{-1} cm^{-1} [IgG; (*15*)] and 84 900 M^{-1} cm^{-1} (FcRn). The extinction coefficient for FcRn in aqueous solution was determined after measurement of the absorbance of the same

† Supported by a Camille and Henry Dreyfuss Teacher Scholar Award (P.J.B.) and a grant from the NIH (AI/GM41239 to P.J.B.).

* Corresponding author. Phone: 626 395-8350. Fax: 626 792−3683. E-mail: bjorkman@cco.caltech.edu.

‡ Division of Biology.

§ Howard Hughes Medical Institute.

⊗ Abstract published in *Advance ACS Abstracts,* July 15, 1997.

[1] Abbreviations: β2m, β_2-microglobulin; EDC, *N*-ethyl-*N*′-[3-(diethylamino)propyl]carbodiimide; FcRn, Fc receptor, neonatal; hu IgG, human immunoglobulin G; IgG, immunoglobulin G; K_D, equilibrium dissociation constant; k_d, dissociation rate constant; mIgG, mouse immunoglobulin G; MHC, major histocompatibility complex; NHS, *N*-hydroxysuccinimide; rmsd, root mean square difference; rIgG, rat immunoglobulin G; RU, resonance units; SPR, surface plasmon resonance.

S0006-2960(97)00841-6 CCC: $14.00

concentration of protein in 6 M GuHCl and phosphate buffered saline (L. M. Sánchez and P.J.B., unpublished results). The reference solution's FcRn concentration was determined from the A_{280} in GuHCl and the theoretical extinction coefficient [valid only for denatured proteins; calculated from the amino acid sequence according to (*16*)].

Immobilization of IgG and FcRn on Biosensor Chips. A BIAcore biosensor system (Pharmacia LKB Biotechnology Incorporated) was used for real time binding experiments. This system includes a biosensor element with a dextran-coated gold surface to which FcRn or IgG was coupled using standard amine coupling chemistry as described in the BIAcore manual. Immobilization of soluble FcRn and IgG proteins using amine coupling chemistry was previously described (*6*−*8*).

Interpretation of Biosensor Data. Binding of soluble IgG or FcRn to the other molecule immobilized on the biosensor chip results in changes in the SPR signal that are directly proportional to the amount of bound protein, and read out in real time as resonance units (RU) (*9*, *10*). Affinities were derived at pH 6.0 by analysis of data obtained from room temperature injections of different concentrations of injected protein in 50 mM phosphate, 150 mM NaCl. Each injection onto an FcRn- or IgG-coupled flowcell was followed by an identical injection onto a blank flowcell of the same chip in order to subtract out significant nonspecific responses.

Two methods were used to derive the equilibrium dissociation constant (K_D). In the first [a Scatchard analysis (*17*)], the slope of the plot of R_{eq}/[ligand] versus R_{eq} is equal to $-1/K_D$ (where R_{eq} is the equilibrium biosensor response and ligand refers to the injected protein). In the second, R_{eq} was plotted versus the log of the concentration of the ligand. Nonlinear regression analysis (*18*) was used to fit these data to a binding model and to derive values for the K_D and the binding response at infinite concentration of ligand (R_{max}). The fit of the data to the following binding models was examined:

(i) A single class of noninteracting binding sites. R_{eq} is represented as

$$R_{eq} = R_{max}([\text{ligand}]/K_D)/(1 + [\text{ligand}]/K_D) \quad (1)$$

(ii) A somewhat more complicated model employing a Hill constant (H) to represent the cooperativity of a class of interacting binding sites. R_{eq} is represented as

$$R_{eq} = R_{max}([\text{ligand}]/K_D)^H/[1 + ([\text{ligand}]/K_D)^H] \quad (2)$$

A Hill constant greater than 1 indicates positive cooperativity; i.e., the binding of one ligand facilitates the binding of additional ligands. A Hill constant less than 1 indicates negative cooperativity; i.e., the presence of a ligand hampers the binding of additional ligands.

(iii) Multiple classes of noninteracting binding sites. R_{eq} is represented as

$$R_{eq} = R_{max}\sum_i f_i\{([\text{ligand}]/K_{D,i})/(1 + [\text{ligand}]/K_{D,i})\} \quad (3)$$

where f_i denotes the fraction of total binding sites in each class and $\sum_i f_i = 1$. (iv) Multiple classes of interacting sites. R_{eq} is represented using eq 3 with the incorporation of Hill coefficients as in eq 2.

For comparison of the models, three statistical parameters were calculated. The correlation coefficient, r^2, is defined as $[\sum_i(x_i - \langle x\rangle)(y_i - \langle y\rangle)]^2/(\sum_i(x_i - \langle x\rangle)^2\sum_i(y_i - \langle y\rangle)^2]$. The rmsd is defined as the root mean square difference between observed and predicted responses for all concentrations tested. The free rmsd was calculated as follows: Data points were omitted one at a time, and a best fit of the model to the remaining data was calculated. For each best fit model, the difference was calculated between the predicted and observed responses for each omitted concentration. The free rmsd is the root mean square of these differences.

For calculation of kinetic constants, the BIAevaluation 2.1 software package was used to fit dissociation curves using a single-exponential dissociation rate equation ($y = R_0e^{-k_d t}$; where R_0 is the observed response at the start of the dissociation and k_d is the dissociation rate constant) or a bi-exponential dissociation rate equation [$y = R_0(f_1e^{-k_{d,1}t} + f_2e^{-k_{d,2}t}$), where $k_{d,1}$ and $k_{d,2}$ represent fast and slow dissociation rate constants and f_1 and f_2 correspond to the fraction of complexes dissociating with each rate constant]. Using the BIAevaluation 2.1 software, an F-test-based comparison between derived χ^2 values for the single-exponential or two-exponential fits yielded an estimated probability for each dissociation curve of which model produced the best fit to the data. In all cases for which two k_d values are reported, the probability that the biexponential model is valid was greater than 0.99. The possibility that the second dissociating population arises from mass transfer effects was ruled out by showing that the dissociation behavior showed no dependence on flow rate (data not shown).

RESULTS

IgG Binding to Immobilized FcRn Fits a Model for Two Noninteracting Classes of Binding Sites. We immobilized FcRn on a biosensor chip and measured the biosensor response at equilibrium (R_{eq}) for the binding of a series of concentrations of a monoclonal IgG. Since large amounts of IgG were needed for injections at high concentrations [and polyclonal rat and mouse IgG bind to rat FcRn with approximately equal affinities (*19*)], we used a mouse monoclonal IgG1 antibody available in the laboratory [1B5 (*13*)].

K_D's are typically derived from biosensor data using a Scatchard plot, in which the slope of the plot of R_{eq}/[injected protein] versus R_{eq} is equal to $-1/K_D$. Determination of binding constants by this method is straightforward for a single class of identical independent sites. However, if there are multiple classes of independent sites or cooperative interactions between sites, the resulting function is nonlinear, and the interpretation is far more complicated. The Scatchard plot for the interaction between immobilized FcRn and the 1B5 IgG shows marked nonlinearity (Figure 1A), as also observed for the FcRn interaction with other IgGs [data not shown; discussed in (*6*, *8*)]. In the previous work, only the data points that correspond to the high-affinity interaction were considered for calculation of the high-affinity K_D.

An alternative method of analysis involves a plot of the equilibrium biosensor response as a function of the log of IgG concentration, and nonlinear regression fitting of these data to a binding model (Figure 1B). This method is preferred over Scatchard analysis for the derivation of binding affinities because (i) the affinity constant is derived using concentrations of protein that bracket the K_D, whereas an affinity can be extrapolated using an inappropriate concentration range in a Scatchard analysis, and (ii) less propagation of experimental error leads to more accurate calculated affinities (*20*).

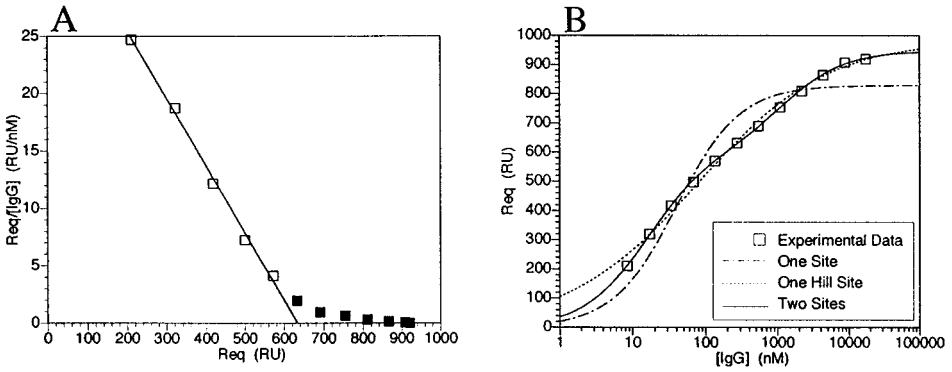

	Best Fit Parameters								Quality of Fit		
Model	$K_{D,1}$ nM	H_1	f_1 %	$K_{D,2}$ μM	H_2	f_2 %	$K_{D,3}$ μM	f_3 %	r^2	rmsd RU	Free rmsd RU
1-Site	40	----	100						0.92	59	71
1-Hill	77	0.49	100						0.994	14	20
2-Site	16	----	63	1.2	----	37			0.9997	3	4
2-Hill	15	1.01	60	1.2	0.88	40			0.9997	3	7
3-Site	15	----	60	1.6	----	30	0.25	9	0.9998	2	4

FIGURE 1: Comparison of Scatchard and nonlinear regression analyses for determining the affinity of IgG binding to immobilized FcRn. FcRn was coupled to a density of 2200 RU (for the experiment shown, and with similar results to densities from 2000 to 4000 RU, data not shown), and 1B5 IgG was injected at the concentrations indicated on the right panel. The same equilibrium binding data are plotted for Scatchard analysis (panel A) and directly as function of IgG concentration (panel B). The Scatchard plot is distinctly nonlinear. The five data points shown as open squares (which correspond to the five lowest IgG concentrations) were used to determine a best fit line from which a high-affinity K_D of 14 nM was derived. The data were also fit using nonlinear regression analysis to five potential binding models. The best fit lines for three of the models are shown; the two most complicated models superimpose closely upon the "Two Sites" model and were omitted for clarity. The best fit parameters and measures of the quality of fit for each of the models, as defined under Materials and Methods, are shown below the plots. The two-site model is the best representation because it is the simplest model that fully accounts for the data.

The binding data were fit to models assuming one, two, or three noninteracting sites and one or two interacting sites. As shown in Figure 1B, the assumption of a single class of binding sites results in a relatively poor fit to the experimental data as judged by the correlation coefficient and rmsd. Adding a Hill coefficient to account for cooperativity among a single class of binding sites improves the fit to the data, but the cooperativity model does not fit the experimental data points as well as a model assuming two classes of noninteracting binding sites. This model predicts the presence of a second lower affinity class of binding sites which are not saturated unless high concentrations of IgG are injected.

More complicated models (three classes of noninteracting binding sites and two classes of cooperative binding sites) also fit the experimental data well. Addition of parameters to a model will usually improve the best fit to the data, therefore resulting in a lower rmsd, but carries the risk of overfitting, i.e., modeling the noise. A model that accurately reproduces the experimental signal should also fit well to data which are excluded while fitting the model parameters (the statistical principle of cross-validation). Using the cross-validation method of testing statistical models (*21*), we calculated a "free rmsd" for each model. The two noninteracting sites model produced both a lower rmsd and a free rmsd than either of the one-site models, demonstrating that the two site model more fully accounts for the data. When two Hill coefficients are included in the two-site model, the rmsd stays the same, but the free rmsd increases slightly, an example of overfitting the data. Addition of a third class of sites yields a slightly lower rmsd compared to the two noninteracting sites model, but a comparable free rmsd, and thus does not significantly improve the fit of the model to the data.

The preceding analyses demonstrate that the interaction of IgG with immobilized FcRn is best represented as two independent classes of IgG binding sites. The class of receptor binding sites with high affinity for IgG is populated at lower IgG concentrations. The derived binding affinity for the high-affinity class of binding sites ($K_{D,1}$ = 16 nM) corresponds to the K_D calculated from a Scatchard analysis when only the points corresponding to the high-affinity interaction are considered [K_D = 14 nM; Figure 1A, and see ref (*6*, *8*)], but the identification of these points is somewhat arbitrary. The second class of binding sites is populated at higher concentrations of IgG. An accurate estimate of the binding affinity of this class of binding sites can only be derived when the concentration range of ligand brackets the K_D, which requires large amounts of IgG (~1 mg per experiment). Under these conditions, the derived binding affinity for the lower affinity class of sites ($K_{D,2}$) is 1.2 μM (Figure 1B).

Kinetic Differences between the Classes of FcRn Binding Sites for IgG. For each concentration of IgG, we analyzed the dissociation of IgG from immobilized FcRn. After the biosensor response reached an equilibrium level, dissociation of IgG was monitored for at least 2 min, and the dissociation phase was analyzed using single and biexponential rate equations. A two-exponential dissociation rate equation fits the data better than a single-exponential rate equation. The fast and slow dissociation rates are sufficiently different to calculate the contribution of each species to the total equilibrium biosensor response for each concentration of IgG. The components of the equilibrium response corresponding to the fast and slow dissociating populations were each fit to a model of one noninteracting binding site, demonstrating that the slow dissociating species binds with a high affinity and the fast dissociating species binds with a lower affinity

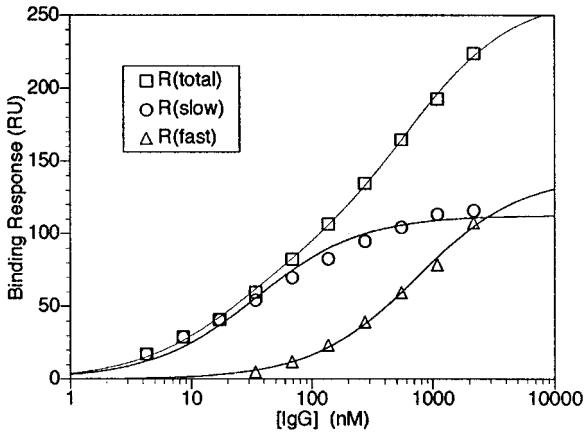

	$K_{D,1}$ nM	$K_{D,2}$ nM
Rtotal	22	650
Rslow	35	
Rfast		740

FIGURE 2: Analysis of the dissociation kinetics for the complex of IgG and immobilized FcRn. FcRn was coupled to a density of 2000 RU, and the dissociation kinetics of FcRn/IgG complexes formed at different IgG concentrations were analyzed. For IgG concentrations above 20 μM, the dissociation kinetics are best represented as a sum of two exponential decays: one with a fast rate constant and the other a slow rate constant. The contributions to the equilibrium response from the fast dissociating population (R_{fast}) and the slow dissociating population (R_{slow}) were determined and plotted as a function of IgG concentration. These data were fit to one-site binding models, and the total equilibrium response (R_{total}) was fit to a two-site model. The derived binding affinities (below panel) show that the slow dissociating population binds with high affinity, and the fast dissociating population binds with low affinity. In order to determine whether the two populations equilibrate independently or one forms from the other, we examined the dissociation behavior after various equilibration periods for a single IgG concentration (2.2 μM). A single concentration of IgG was passed over immobilized FcRn and allowed to bind for various times. The total response at the time of dissociation was measured, and the components of this response dissociating with fast and slow kinetics were calculated. The biosensor response for each population is relatively constant for each equilibration period, supporting the hypothesis that the two populations of complexes equilibrate independently (data not shown).

(Figure 2). Thus, both the equilibrium measurements and the dissociation kinetics are consistent with two populations of FcRn/IgG complexes: a high-affinity, slow dissociating species; and a low-affinity, fast dissociating species.

Since most previous determinations of FcRn binding affinities included an equilibration step followed by a washing step [e.g., (*12, 22, 23*)], we examined the dependence of the observed affinity on the duration of a washing step. Different concentrations of IgG were passed over immobilized FcRn, and the response was measured at equilibrium, and at 30, 60, and 600 s into the dissociation phase (Figure 3A). The equilibrium data were fit to a model of two independent binding sites. The other curves were fit assuming the values derived at equilibrium for the high- and low-affinity binding constants. Because the low-affinity complex dissociates faster, the fraction of IgG bound to the high-affinity class of binding sites increases with washing time. Indeed, after 10 min of washing, the fraction of complexes in the low-affinity class becomes negligible, and the data can be modeled as a single class of noninteracting binding sites (Figure 3B; Scatchard plots of these data become progressively more linear with increased washing time). We conclude that experiments which include room temperature washing steps of several minutes or longer would not detect either the biphasic nature of equilibrium Scatchard plots or the presence of a low-affinity class of binding sites.

High-Affinity Binding of FcRn to IgG Requires Receptor Immobilization. In previous studies of the interaction between FcRn and IgG, we noted differences in binding affinities depending on which species was immobilized on the biosensor surface (*7, 8*). In order to characterize these differences, we immobilized the IgG used for the previous experiments (1B5) on the biosensor surface, and measured the equilibrium binding response for various concentrations of soluble FcRn (Figure 4). A best fit for each of the previously discussed five models was calculated. Using the criteria outlined above, the data are best modeled as two classes of independent FcRn binding sites on immobilized IgG. Comparing the affinities calculated for IgG immobilized to those calculated for FcRn immobilized demonstrates that, while the low-affinity binding constants are similar ($K_{D,2}$ = 2.4 μM for IgG immobilized; $K_{D,2}$ = 1.2 μM for FcRn immobilized), the high-affinity class of binding sites interacts more weakly when IgG is immobilized ($K_{D,1}$ = 210 nM for IgG immobilized; $K_{D,1}$ = 16 nM for FcRn immobilized). The dissociation kinetics for the FcRn interaction with IgG immobilized were also examined. As was the case with FcRn immobilized, the dissociation behavior is better modeled as two independently dissociating complexes than as a single species. Consistent with the comparison of the equilibrium binding results, the slow dissociating species dissociates faster when IgG rather than FcRn is immobilized ($k_{d,1} \geq 0.01$ s^{-1} for IgG immobilized; $k_{d,1}$ from 0.002 to 0.0002 s^{-1} for FcRn immobilized), while the fast dissociation rates are similar ($k_{d,2} \geq 0.01$ s^{-1} for either IgG or FcRn immobilized).

In order to examine if the difference in the affinity of the high-affinity class of binding sites generally depends on which species is immobilized, we did a systematic study of the binding interactions of nine different IgG molecules at pH 6.0, and derived K_D values corresponding to the high-affinity class of sites. For each monoclonal antibody, separate experiments were conducted with the antibody immobilized and with the receptor immobilized. For the interaction of each antibody with FcRn, the dissociation rate is slower and the affinity is higher when FcRn, rather than the IgG, is immobilized (Table 1). Because we see this effect for all of the IgG molecules tested, we conclude that these observed diffenences in affinity are a general property of the IgG/FcRn interaction.

Comparison of the Interaction of FcRn with IgG versus Fc. The binding site for FcRn is located within the Fc region of IgG, but the effects of including the F_{ab} arms of an intact antibody upon the FcRn interaction with Fc have not been systematically analyzed using biosensor technology. We therefore compared binding of several sets of IgGs and their corresponding Fc fragments to immobilized FcRn (Table 2). In each case, the binding data reveal the existence of high- and low-affinity populations of FcRn. The affinities and dissociation rates for IgG and Fc binding are similar, although high-affinity ($K_{D,1}$) FcRn/IgG complexes are slightly weaker interacting than the high-affinity FcRn/Fc complexes. This effect could be entropic (due to constraint of the IgG F_{ab} arms upon FcRn binding) and/or because the bulky F_{ab} arms interact unfavorably with FcRn. $k_{d,1}$ is faster for the Fc fragments (by a factor of $\sim$2) than for the corresponding intact antibodies. The combination of faster dissociation rates and higher affinities for the high-affinity FcRn/Fc

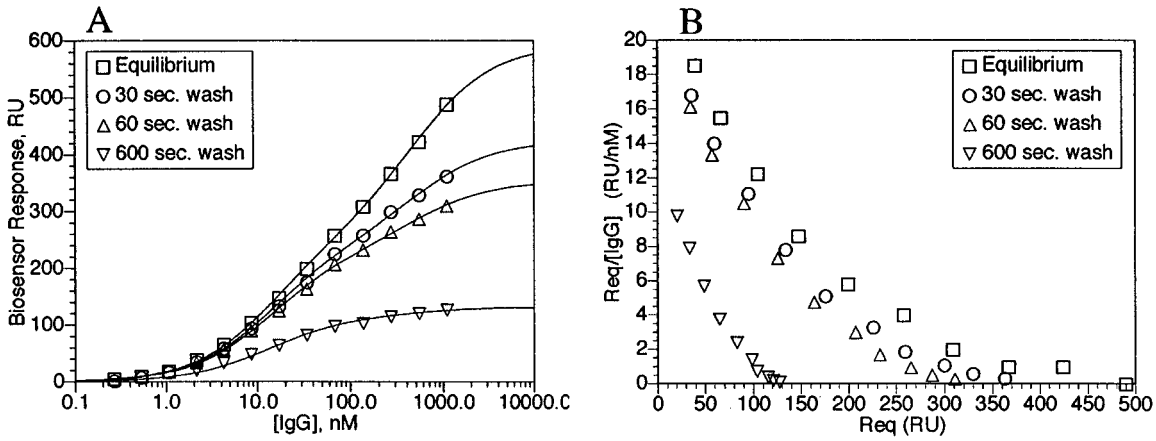

	$K_{D,1}$ nM	f_1 %	$K_{D,2}$ nM	f_2 %	R_{max} RU
R_{eq}	14	42	470	58	590
$R_{30\ sec}$	14	56	470	44	430
$R_{60\ sec}$	14	64	470	36	360
$R_{600\ sec}$	14	88	470	12	140

FIGURE 3: Effect of washing time on observed IgG affinity for immobilized FcRn. FcRn was coupled to a density of 2200 RU, and various concentrations of 1B5 IgG were injected. The biosensor response at equilibrium and after various washing durations is plotted as a function of concentration for the interaction of IgG with immobilized FcRn (panel A). The equilibrium data were best fit to a two site binding model. The curves representing experiments employing washing steps of 30, 60, or 600 s were fit to a two-site model constrained to the binding affinities determined using the equilibrium data. Because the low-affinity population dissociates with faster kinetics (Figure 2 and text), the washing step selectively depopulates the low-affinity site. Although biosensor methods allow equilibrium binding to be measured directly, many other methods employ a washing time of several minutes. For washing times of 10 min or longer, the Scatchard plots of these data (panel B) become essentially linear, and the existence of a low-affinity state would be missed.

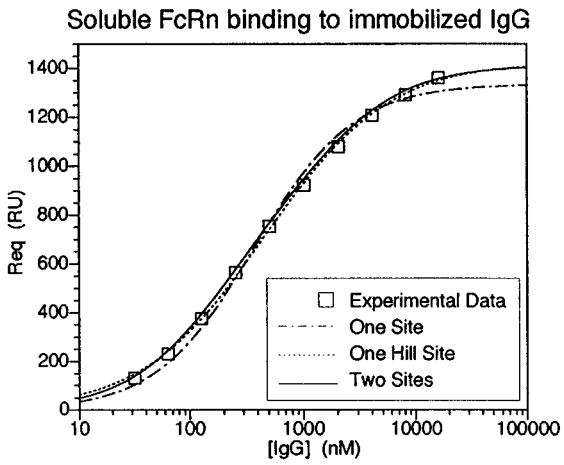

	Best Fit Parameters								Quality of Fit		
Model	$K_{D,1}$ nM	H_1	f_1 %	$K_{D,2}$ μM	H_2	f_2 %	$K_{D,3}$ μM	f_3 %	r^2	rmsd RU	Free rmsd RU
1-Site	370	—	100						0.994	36	47
1-Hill	460	0.80	100						0.9993	12	18
2-Site	210	—	66	2.4	—	34			0.99995	3	6
2-Hill	140	1.63	15	0.7	0.74	85			0.99997	2	6
3-Site	203	—	56	1.9	—	31	100*	13	0.99996	3	21

FIGURE 4: Soluble FcRn binding to immobilized IgG. 1B5 IgG was immobilized to a density of 3700 RU (for the experiment shown, and with similar results to densities from 1300 to 13000 RU, data not shown), and various concentrations of FcRn were injected. The biosensor response at equilibrium is plotted as a function of the concentration of IgG. Five binding models (see Figure 1) were fit to the data; again, the two-site model best represents the data. Asterisk: the third binding affinity in the three site model was fixed at 100 μM. Without constraint, this affinity and the corresponding R_{max} both increased toward infinity.

interaction compared to the high-affinity FcRn/IgG interaction implies that Fc fragment association rates must be faster (by a factor of ~4).

DISCUSSION

To achieve high-affinity binding comparable to that observed for cell surface FcRn, we find that the receptor, rather than its ligand, must be immobilized on the biosensor chip. Previously reported binding affinities for the interaction of IgG with rat FcRn on the surface of brush border, intestinal, or transfected cells are in the range of $K_D = 8-55$ nM (*7*, *12*). In the present study, we observe affinities ranging from 17 to 93 nM for a series of soluble IgGs binding to immobilized FcRn. For the complementary interaction, soluble FcRn interacting with the same IgGs, we consistently observed a lower affinity and faster dissociating class of

Table 1: Dependence of the High-Affinity Binding Mode on the Species Immobilized[a]

	FcRn immobilized		IgG immobilized	
	$K_{D,1}$ (nM)	$k_{d,1}$ (10^{-3} s^{-1})	$K_{D,1}$ (nM)	$k_{d,1}$ (10^{-3} s^{-1})
mIgG1	22	1.9	250	30
mIgG2a	39	0.5	370	20
mIgG2b	41	0.2	260	40
rIgG1	34	0.7	180	40
rIgG2a	15	0.3	80	10
rIgG2b	93	0.7	*	*
rIgG2c	84	1.3	740	20
anti-CD4 (rIgG2a)	24	0.5	74	30
1B5 (mIgG1)	17	1.0	210	10

[a] Equilibrium dissociation constants and dissociation rate constants are reported for the interaction of FcRn with monoclonal IgGs. For each IgG studied, either FcRn or the IgG was coupled to the biosensor surface. FcRn was coupled to a density of 2600 RU (and several concentrations between 2000 and 4000 RU for the 1B5 measurements). The same protocol was followed for coupling each IgG, resulting in densities between 500 and 7000 RU (*: rIgG2b was not coupled successfully with this protocol). Regardless of the coupling density, in each case in which IgG is immobilized, the high-affinity interaction is weaker and shows faster dissociation kinetics than the corresponding interaction when FcRn is immobilized. Only the high-affinity K_D values are reported for these experiments. The low-affinity K_D's could not be accurately determined because the quantities of most of the IgGs were limited, and we were not able to assay equilibrium binding at the high concentrations required to saturate the low-affinity binding mode. As can be seen by the close agreement of high affinity binding constants derived from three independent assays of 1B5 binding to immobilized FcRn (Figures 1−3), the high-affinity binding mode can be accurately measured in experiments in which the low-affinity mode is not saturated. The equilibrium and kinetic constants reported for 1B5 binding to immobilized FcRn are the average of the three experiments involving 1B5 presented in this paper.

Table 2: Comparison of Binding Affinities of Intact IgGs and Corresponding Fc Fragments for Immobilized FcRn[a]

	$K_{D,1}$ (nM)	$k_{d,1}$ (10^{-3} s^{-1})
3F4 IgG (mIgG1)	49	0.6
3F4 Fc	11	2.5
Hu IgG (polyclonal)	15	0.5
Hu Fc	9.7	0.9
Rat IgG (polyclonal)	4.1	0.6
Rat Fc	1.5	1.3

[a] FcRn was coupled to a biosensor chip to a density of 2600 RU. Affinities were derived for a two-site binding model by nonlinear regression analysis. Rate constants reported are an average for all concentrations of IgG injected.

binding sites (Table 1). The weaker affinities of immobilized IgGs for FcRn are comparable to the 500 nM K_D obtained by isothermal titration calorimetry for the interaction of soluble FcRn with human IgG (*14*). We conclude that FcRn must be constrained to some sort of two-dimensional surface (a membrane or a biosensor chip) to achieve high-affinity binding of IgG. In vivo, FcRn is an integral membrane protein that interacts with soluble IgGs; therefore, the interaction of immobilized FcRn with soluble IgG should be more representative of physiological conditions than the reverse situation (immobilized IgG interacting with soluble FcRn). In the study of the interaction between cholera toxin and gangliosides, it was also noted that biosensor analyses with the normally membrane-associated gangliosides immobilized reproduced whole cell assays more closely than free solution measurements, presumably because the biosensor measurements were performed on surfaces resembling the cell membrane (*24*).

Several previous studies support the hypothesis that two FcRn molecules dimerize, as observed in FcRn and FcRn/Fc crystals (*3, 25*), to form the high-affinity binding site for a single IgG. A 2:1 receptor:ligand stoichiometry was observed for rat FcRn interacting with IgG in solution and in crystals of the receptor/Fc complex (*14, 25*). Site-directed FcRn mutants with alterations that specifically affect the interaction of IgG with FcRn dimers, but not with monomers, show reduced affinities in biosensor assays and in measurements of labeled IgG binding to cell surface FcRn (*7*). Finally, the role of FcRn dimerization in its interaction with IgG was directly tested by introducing cysteines at positions that either facilitated or hindered receptor dimerization when FcRn was coupled to a biosensor chip using thiol chemistry (*8*). High-affinity binding (K_D = 22 nM) was observed when FcRn was coupled in the orientation facilitating dimerization, but the binding affinity was reduced to a $K_D > 4$ μM when receptor dimerization was hindered. In the present study, the K_D values derived for the high-affinity population of immobilized FcRn are similar to those observed for dimerization-facilitated FcRn (*8*), implying that the high-affinity population represents IgG bound to receptor dimers. When FcRn is immobilized on a biosensor chip, it is attached to a long flexible dextran moiety at concentrations $\geq\sim$100 μM (*26*). This FcRn concentration is much higher than the concentration of soluble FcRn interacting with immobilized IgG, and therefore the equilibrium between monomeric and dimeric FcRn will be shifted to include a larger fraction of dimer when FcRn is immobilized. Immobilization of FcRn also reduces the loss of entropy associated with dimerization, the major energetic hindrance to dimerization (*27*). The entropy of the monomer and of the dimer is reduced upon immobilization to the dextran molecules because some of their rotational and translational movements are restricted. Since the loss of entropy upon immobilization occurs twice for monomers but only once for a dimer, the loss of entropy upon dimerization is lower for immobilized FcRn than for soluble FcRn. Both of these effects promoting dimerization (higher local concentration and reduction in the loss of entropy) should increase the affinity for IgG for both membrane-associated FcRn and FcRn immobilized on a biosensor chip relative to the IgG affinity of soluble FcRn.

Previous biosensor analyses of the interaction of immobilized FcRn with IgG were complicated by nonlinear behavior in Scatchard analyses (*6, 8*). Here we show that two classes of noninteracting FcRn/IgG complexes are sufficient to explain this nonlinear behavior, and characterize them as a slow dissociating population with a similar affinity to the range of values calculated in studies using membrane-bound FcRn (*7, 12*), and a fast dissociating population with lower affinity. We have shown that it is the high-affinity mode that depends on which species is immobilized.

The low-affinity ($K_{D,2}$) fast dissociating ($k_{d,2}$) binding component is similar with either IgG or FcRn immobilized. This binding mode could exist under physiologically relevant conditions or could result from some specific property of the biosensor analysis. Characteristics of biosensor methodology that have been proposed to potentially alter a binding interaction include mass transfer properties of the soluble ligand and effects on the receptor due to its immobilization (*26, 28, 29*). Mass transfer considerations are important when evaluating kinetic data but irrelevant under equilibrium

conditions. Since the low-affinity populations are observed under equilibrium conditions, they cannot result from mass transfer effects. It is unlikely that the low-affinity FcRn population is an artifact of the amine coupling method because kinetic analysis revealed two classes of IgG binding sites for FcRn immobilized by thiol coupling methods (*8*). Using any coupling chemistry, steric hindrance of one immobilized FcRn molecule by another and/or occlusion of unoccupied binding sites by bound IgG molecules could introduce nonideal binding behavior. However, the excellent agreement of the equilibrium binding response to a two-site model suggests that this is not a significant effect in our case. If the low affinity-binding mode is not biosensor specific, then a population of FcRn molecules with low affinity for IgG could exist under physiological conditions. However, it would be difficult to detect on biological membranes because the techniques used to measure this interaction generally require a washing step that is long relative to the dissociation rate of the low-affinity complexes, and would therefore result in nearly complete dissociation of these complexes (Figure 3). Regardless of the origin of the low-affinity population, we can separate the contributions of the high- and low-affinity binding interactions. Therefore, our observations about the high-affinity binding mode are independent of the existence of a low-affinity mode.

Biosensor-based methods have been used to study the interaction between FcRn and IgG (*6*−*8*, *30*), and these characterizations agree well with the results from *in vivo* and cell binding studies (*7*, *12*, *31*, *32*). Some of the lessons we have learned in our studies may be relevant in other biosensor-based investigations. We have calculated binding constants using equilibrium rather than kinetic data because the latter can lead to incorrect results if the data are mass transfer limited or the reaction mechanism is unknown (*26*, *28*, *29*). In these analyses, we used a best fit procedure that optimizes the agreement between the observed and modeled equilibrium binding response equally for all concentrations of ligand. This method is preferable to Scatchard analyses which overemphasize the poorly determined weaker binding responses. The use of cross-validation, which has been widely used in the refinement of crystallographically-derived protein structures (*33*), allowed us to detect instances in which the addition of extra parameters resulted in overfitting the data by modeling noise rather than the signal. This method should be generally applicable for biosensor analyses. The significant differences in affinities we observe depending on which species is immobilized highlight the importance of characterizing a binding interaction in both orientations. Finally, for the special case of two noninteracting populations of binding sites with different dissociation rates, utilization of the dissociation phase of the measurement, either by delayed sampling or by modeling the dissociation phase and treating the components of the total response separately, could allow characterization of each population of binding sites.

ACKNOWLEDGMENT

We thank Luis Sánchez for providing purified monoclonal antibodies, Malini Raghavan and Robert Karlsson for helpful discussions, and members of the laboratory for critical reading of the manuscript.

REFERENCES

1. Junghans, R. P. (1997) *Immunol. Res. 16*, 29−57.
2. Simister, N. E., and Mostov, K. E. (1989) *Nature 337*, 184−187.
3. Burmeister, W. P., Gastinel, L. N., Simister, N. E., Blum, M. L., and Bjorkman, P. J. (1994) *Nature 372*, 336−343.
4. Gastinel, L. N., Simister, N. E., and Bjorkman, P. J. (1992) *Proc. Natl. Acad. Sci U.S.A. 89*, 638−642.
5. Rodewald, R., and Kraehenbuhl, J.-P. (1984) *J. Cell Biol. 99*, S159−S164.
6. Raghavan, M., Bonagura, V. R., Morrison, S. L., and Bjorkman, P. J. (1995) *Biochemistry 34*, 14649−14657.
7. Raghavan, M., Chen, M. Y., Gastinel, L. N., and Bjorkman, P. J. (1994) *Immunity 1*, 303−315.
8. Raghavan, M., Wang, Y., and Bjorkman, P. J. (1995) *Proc. Natl. Acad. Sci. U.S.A. 92*, 11200−11204.
9. Fägerstam, L. G., Frostell-Karlsson, A., Karlsson, R., Persson, B., and Rönnber, I. (1992) *J. Chromatogr. 597*, 397−410.
10. Malmqvist, M. (1993) *Nature 361*, 186−187.
11. Raghavan, M., and Bjorkman, P. J. (1995) *Structure 3*, 331−333.
12. Mackenzie, N. (1984) *Immunol. Today 5*, 364−366.
13. Sánchez, L. M., López-Otín, C., and Bjorkman, P. J. (1997) *Proc. Natl. Acad. Sci. U.S.A. 94*, 4626−4630.
14. Huber, A. H., Kelley, R. F., Gastinel, L. N., and Bjorkman, P. J. (1993) *J. Mol. Biol. 230*, 1077−1083.
15. Fasman, G. D. (1989) *Practical Handbook of Biochemistry and Molecular Biology*, p 265, CRC Press, Inc., Boca Raton, FL.
16. Gill, S. C., and Von Hippel, P. H. (1989) *Analy. Biochem. 182*, 319−326.
17. Scatchard, G. (1949) *Ann. N.Y. Acad. Sci. 51*, 660−672.
18. Press, W. H., Teukolsky, S. A., Vetterling, W. T., and Flannery, B. P. (1992) *Numerical recipes in Fortran. The art of scientific computing* 2nd ed., pp 678−683, Cambridge University Press, New York.
19. Huber, A. H. (1994) *A biochemical and structural characterization of Drosophila neuroglian*, Thesis, California Institute of Technology.
20. Weber, G. (1992) *Protein Interactions*, Routledge, Chapman, and Hall, Inc., New York.
21. Efron, B., and Tibshirani, R. (1991) *Science 253*, 390−395.
22. Wallace, K. H., and Rees, A. R. (1980) *Biochem. J. 188*, 9−16.
23. Rodewald, R., Lewis, D. M., and Kraehenbuhl, J. P. (1983) in *Brush Border Membranes (Ciba Found. Symp. 95)*, p 287, Pitman Books Ltd., London.
24. Kuziemko, G. M., Stroh, M., and Stevens, R. C. (1996) *Biochemistry 35*, 6375−6384.
25. Burmeister, W. P., Huber, A. H., and Bjorkman, P. J. (1994) *Nature 372*, 379−383.
26. Karlsson, R., Roos, H., Fägerstrom, L., and Persson, B. (1994) *METHODS*: *Compan. Methods Enzymol. 6*, 99−110.
27. Finkelstein, A. V., and Janin, J. (1989) *Protein Eng. 3*, 1−3.
28. Schuck, P., and Minton, A. P. (1996) *Trends Biochem. Sci. 21*, 458−460.
29. O'Shannessy, D. J. (1996) *Anal. Biochem. 236*, 275−283.
30. Popov, S., Hubbard, J. G., Kim, J.-K., Ober, B., Ghetie, V., and Ward, E. S. (1996) *Mol. Immunol. 33*, 521−530.
31. Kim, J.-K., Tsen, M.-F., Ghetie, V., and Ward, E. S. (1994) *Eur. J. Immunol. 24*, 2429−2434.
32. Kim, J.-K., Tsen, M.-F., Ghetie, V., and Ward, E. S. (1994) *Scand. J. Immunol. 40*, 457−465.
33. Brünger, A. T. (1992) *Nature 355*, 472−475.

BI970841R